Biochemical Pharmacology 77 (2009) 1642–1654

Contents lists available at ScienceDirect

Biochemical Pharmacology

journal homepage: www.elsevier.com/locate/biochempharm

In vitro studies on the metabolism of trabectedin (YONDELIS®) in monkey and man, including human CYP reaction phenotyping

Marc Vermeir [a,1,*], Alex Hemeryck [a,1,2], Filip Cuyckens [a], Andres Francesch [b], Marc Bockx [a], Jos Van Houdt [a], Kathleen Steemans [a], Geert Mannens [a], Pablo Avilés [b], Roland De Coster [a]

[a] Johnson & Johnson Pharmaceutical Research and Development (J&JPRD), A Division of Janssen Pharmaceutica N.V., Turnhoutseweg 30, B-2340 Beerse, Belgium
[b] PharmaMar, Avenida de los Reyes 1, Pol. Ind. La Mina-Norte, E-28770 Colmenar Viejo, Madrid, Spain

ARTICLE INFO

Article history:
Received 6 January 2009
Accepted 23 February 2009

Keywords:
Trabectedin
In vitro metabolism
Human
Monkey
CYP reaction phenotyping

ABSTRACT

Trabectedin (YONDELIS®) is a potent anticancer agent which was recently approved in Europe for the treatment of soft tissue sarcoma. The drug is currently also in clinical development for the treatment of ovarian carcinoma. *In vitro* experiments were conducted to investigate the hepatic metabolism of [^{14}C]trabectedin in Cynomolgus monkey and human liver subcellular fractions. The biotransformation of trabectedin was qualitatively similar in 12,000 × *g* supernatants of both species, and all human metabolites were also produced by the monkey. The trabectedin metabolites were identified by QTOF mass spectrometry, and HPLC co-chromatography with reference compounds. Trabectedin was metabolized via different biotransformation pathways. Most of the metabolic conversions occurred at the trabectedin A domain including mono-oxidation and di-oxidation, carboxylic acid formation with and without additional oxidation, and demethylation either without (*N*-demethylation to ET-729) or with additional mono-, di- or tri-oxidation. Another metabolite resulted from *O*-demethylation at the trabectedin C subunit, and in addition, aliphatic ring opening of the methylene dioxybridge at the B domain was detected. Overall, demethylation and oxidation played a major role in phase I metabolism of the drug. Human cDNA expressed CYPs 1A2, 2A6, 2B6, 2C8, 2C9, 2C18, 2D6, 2E1, 3A4 and 3A5 in *E. coli* membranes, but not CYP1B1, 2C19, and 4A11 were able to metabolize [^{14}C]trabectedin. Experiments with chemical inhibitors and CYP inhibitory antibodies indicated that, at therapeutic levels, CYP3A4 is the main human CYP isoform involved in trabectedin's hepatic metabolism. In monkey and human liver microsomes, trabectedin was not substantially metabolized by glucuronidation.

1. Introduction

Trabectedin (YONDELIS®, previously known as ecteinascidin-743 or ET-743) is a marine alkaloid originally isolated from the Caribbean tunicate *Ecteinascidia turbinata*. Its chemical structure is characterized by three fused tetrahydroisoquinoline subunits (Fig. 1). Subunits A and B are fused into a monobridged pentacyclic skeleton. Subunit C is linked to the A-B core via a ten membered lactone bridge through a benzylic sulfide linkage. Trabectedin binds covalently to guanine residues in the minor groove of the DNA double helix, triggering a cascade of events which include interference with several transcription factors, DNA binding proteins and repair pathways, and disruption of the cell cycle. This results in potent antitumor activity against a number of cell lines *in vitro*, and important antiproliferative effects *in vivo* against a variety of experimental tumors [1].

In clinical trials, single agent trabectedin has shown activity in soft tissue sarcoma, breast, prostate and ovarian carcinomas [1–3]. Recently, intravenous trabectedin has been approved in Europe for use in patients with advanced soft tissue sarcoma after failure of antracyclines or ifosfamide, or who are unsuited to receive these agents [4]. Several clinical trials are currently ongoing to further substantiate its clinical activity either as a single agent or in combination with other anticancer agents [4] (see also: http://www.clinicaltrials.gov).

Despite the long standing clinical use of YONDELIS®, the metabolism of trabectedin remains largely unknown. Attempts to elucidate the compound's metabolism in *in vitro* systems [5,6] were only partially successful. Sparidans et al. [5] identified a few metabolites and degradation products in human liver microsomes. Reid et al. [6] identified three oxidative metabolites in cDNA-expressed CYP systems. The metabolic fate of trabectedin *in vivo*

* Corresponding author at: Department of Preclinical Pharmacokinetics, Global Preclinical Development, J&JPRD, A Division of Janssen Pharmaceutica N.V., Turnhoutseweg 30, B-2340 Beerse, Belgium. Tel.: +32 14.60.52.97; fax: +32 14.60.51.10.
E-mail address: mvermeir@its.jnj.com (M. Vermeir).
[1] Equal contributions were made by these authors.
[2] Current address: Ablynx N.V., Technologiepark 4, B-9052 Zwijnaarde, Belgium.

0006-2952/$ – see front matter © 2009 Elsevier Inc. All rights reserved.
doi:10.1016/j.bcp.2009.02.020

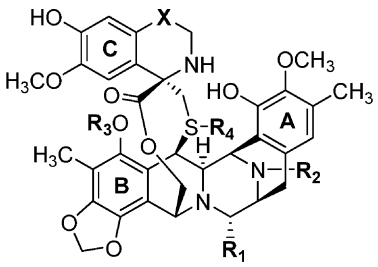

	R_1	R_2	R_3	R_4	X
Trabectedin (ET-743)	OH	CH_3	CH_3CO	-	CH_2
[^{14}C]Trabectedin	OH	CH_3	CH_3CO	-	$^{14}CH_2$
ET-701	OH	CH_3	H	-	CH_2
ET-729	OH	H	CH_3CO	-	CH_2
ET-745	H	CH_3	CH_3CO	-	CH_2
ET-759A	=O	CH_3	CH_3CO	-	CH_2
ET-759B	OH	CH_3	CH_3CO	=O	CH_2

Fig. 1. Chemical structure of trabectedin and authentic reference compounds used for HPLC co-chromatography. The three domains, A–B–C, of trabectedin are indicated.

has neither been well characterized [1,7,8]. Beumer et al. [8] reported on the metabolite profiling in urine and faeces samples from cancer patients after intravenous administration of [^{14}C]trabectedin. A large number of metabolites were detected, however, only a few putative metabolites were tentatively identified [8]. The incomplete knowledge on trabectedin's *in vivo* metabolism may in part be explained by the fact that *in vivo* investigations are seriously hampered by several compound related factors, including the low dose, the complexity of metabolism and the extremely low metabolite concentrations [5,7,8].

In vitro metabolism studies using [^{14}C] labelled trabectedin and hepatic subcellular fractions of various species have shown that the *in vitro* metabolic profile of man and monkey were qualitatively similar, whilst that of other species including rat and dog was quite different [9]. Although these investigations provided a preliminary comparative metabolic profile across species, additional studies were needed to further substantiate the similarity between human and Cynomolgus monkey hepatic metabolism including characterization of biotransformation pathways and the identity of trabectedin metabolites. Species-differences in trabectedin metabolism are of particular relevance to the preclinical safety evaluation of trabectedin-induced hepatotoxicity, whose nature has been shown to be species-dependent [7].

During preclinical risk assessment, results from *in vitro* and/or *in vivo* metabolism studies can assist in the selection of appropriate animal species for toxicological assessments [10,11]. In addition to the species selection for preclinical risk assessment, the prediction of metabolism-based drug–drug interactions is another important aspect during drug development [12,13]. This is particularly relevant to anti-cancer agents as the target populations for these drugs are at considerable risk of drug–drug interactions [14–16]. The characterization of a compound's elimination pathways including the enzyme(s) responsible for its metabolism typically forms the basis to assess whether a drug may be the precipitant of a metabolism-based drug interaction [12,13]. *In vitro* investigations using human hepatic subcellular fractions and heterologously expressed human CYP (cytochrome P-450) forms have indicated that virtually all major CYPs are able to metabolize trabectedin [5,6], but that CYP3A4 is likely the major isoform [17].

The aims of the present *in vitro* studies were therefore twofold: first, to elucidate the metabolism of trabectedin in hepatic subcellular fractions of the Cynomolgus monkey and man, second, to delineate the involvement of CYP in trabectedin's human metabolism.

2. Materials and methods

2.1. Chemicals

Radiolabelled [^{14}C]trabectedin (Fig. 1) with a specific activity of 2.02 MBq/mg and a radiochemical purity of 92.7% was synthesized at PharmaMar (Colmenar Viejo, Madrid, Spain). Unlabelled trabectedin of natural source (chemical purity of 98.8%), tri-deuterated trabectedin and unlabelled authentic reference compounds (Fig. 1) used for HPLC co-chromatography were kindly provided by PharmaMar. The chemical inhibitors used in the CYP phenotyping experiments were obtained from the following sources: furafylline (Ultrafine Chemicals, Manchester, UK); 8-methoxypsoralen, quinidine and ketoconazole (Janssen Chimica, Geel, Belgium); trimethoprim and sulfaphenazole (Sigma–Aldrich, St.-Louis, MO, USA); diethyldithiocarbamate (Merieux, Lyon, France); troleandomycin (Pfizer, New York, NY, USA) and (±)-3-benzyl-phenobarbital (Synthesis BA/DMPK department of J&JPRD). Glucose-6-phosphate dehydrogenase, glucose-6-phosphate and NADP were obtained from Roche Diagnostics (Mannheim, Germany). All other chemicals were of the highest quality commercially available.

2.2. Biological reagents

For the *in vitro* metabolism experiments, pooled batches of human liver subcellular fractions were prepared from liver tissue obtained from male and female human kidney transplant donors ($n = 4$). For the incubations with liver subcellular fractions of male Cynomolgus monkey, two pools ($n = 3$ and $n = 4$) purchased from Biopredic International (Rennes, France), were combined.

The pooled human liver microsomes ($n = 38$) used for the CYP phenotyping experiments were obtained from BD Biosciences (San Jose, CA, USA). For the preparation of cDNA-expressed human P450 enzyme systems, constructs in *E. coli* cells [18,19] were obtained from the Biomedical Research Centre, Ninewells Hospital, Dundee (UK) via the Link project 1994–1998 (a program of the University of Dundee/Biotechnology and Biology Research Council/Department of Trade and Industry/Pharmaceutical Industry). Membranes of recombinant *E. coli* systems expressing individual CYPs (CYP1A2, CYP1B1, CYP2A6, CYP2B6, CYP2C8, CYP2C9, CYP2C18, CYP2C19, CYP2D6, CYP2E1, CYP3A4, CYP3A5, or CYP4A11) and NADPH-P450 reductase were prepared at the BA/DMPK department of J&JPRD using published procedures [20,21].

Purified inhibitory monoclonal antibodies against human CYP1A2, CYP2A6, CYP2B6, CYP2C8, CYP2C9, CYP2C19, CYP2D6

and CYP2E1, and Control IgG (pre-immune IgG from rabbit) were obtained from XenoTech LLC (Lenexa, Kansas, USA). Monoclonal antibody inhibitory to CYP3A4 was purchased from BD Biosciences (San Jose, CA, USA).

Human liver subcellular fractions were prepared following standard procedures [22,23]. Protein and cytochrome P450 concentrations were determined according to the methods of Lowry [24] and Omura and Sato [25], respectively.

2.3. Trabectedin metabolism in liver subcellular fractions

For the incubations with hepatic subcellular fractions, 1-mM stock solutions of [^{14}C]trabectedin in DMSO (radioactivity concentration of 1.08 MBq/ml) were prepared. The stock solutions of [^{14}C]trabectedin were prepared immediately before the incubations, in order to minimize chemical degradation. The incubations were carried out in a total volume of 2 ml at a final [^{14}C]trabectedin concentration of 5 μM (5.4 kBq/ml) for 120 min at 37 °C under continuous shaking at 100 oscillations/min. Final solvent concentrations were 0.5% (v/v). To examine phase I metabolism, incubations of [^{14}C]trabectedin with hepatic 12,000 × *g* supernatant fractions (equivalent to 1 and 2 mg/ml microsomal protein for human and monkey samples, respectively) were performed in 0.25 M Na, K-phosphate buffer pH 7.4 in the presence of a NADPH-generating system (1 mg of glucose-6-phosphate, 0.5 units of glucose-6-phosphate dehydrogenase, 1 mg of $MgCl_2{\cdot}6H_2O$ and 0.25 mg of NADP). To investigate phase II metabolism (glucuronidation), incubations of [^{14}C]trabectedin with human and monkey liver microsomes were performed at a protein concentration of 1 mg/ml in the presence of UDPGA (5 mM), $MgCl_2.6H_2O$ (100 mM) and saccharolactone (5 mM) in 50 mM Tris–HCl buffer pH 7.5. Saccharolactone was included as β-glucuronidase inhibitor. After a 5 min preincubation, the reactions were started by addition of the radiolabelled compound. The incubations were terminated by snapfreezing the samples in dry ice. Boiled liver subcellular fractions, incubated during 120 min under identical conditions, served as controls to assess the chemical stability of trabectedin. The samples were stored at or below −18 °C until analysis.

2.4. CYP phenotyping

Incubations of [^{14}C]trabectedin with recombinant CYP enzymes co-expressed with NADPH-P450 reductase in *E. coli* membranes were performed under the same incubation conditions as for the metabolism experiments with liver 12,000 × *g* supernatant fractions. The incubations were carried out at a cytochrome P450 concentration of 200 pmol/incubate. Vector controls without expressed human monooxygenase enzymes were run in parallel to the test samples.

For the incubations with CYP-specific chemical inhibitors and inhibitory antibodies, unlabelled trabectedin was dissolved in DMSO to a concentration of 2 μg/ml. The chemical inhibitors were dissolved in methanol, except for quinidine which was dissolved in water. Incubations of unlabelled trabectedin (10 ng/ml) with human liver microsomes (0.1 mg/ml) and a NADPH-generating system (see before, with omission of NADP) in the presence of the CYP-specific chemical inhibitors [13,26] were performed at single inhibitor concentrations (inhibitable CYPs given between brackets) viz. 10 μM furafylline (CYP1A2), 2.5 μM 8-methoxypsoralen (CYP2A6), 100 μM trimethoprim (CYP2C8), 10 μM sulfaphenazole (CYP2C9), 1 μM 3-benzyl-phenobarbital (CYP2C19), 3 μM quinidine (CYP2D6), 100 μM diethyldithiocarbamate (CYP2E1), 1 μM ketoconazole (CYP3A4/5) and 200 μM troleandomycin (CYP3A4/5). Final solvent concentrations were ≤1% (v/v). After a 5 min preincubation, NADP (0.125 mg) was added to a final volume of 1 ml and the samples were incubated for 0, 5, 10, 15 and 20 min. For the mechanism-based inhibitors, the microsomes were preincubated with the inhibitors (5, 10, 15 and 30 min for 8-methoxypsoralen, furafylline, diethyldithiocarbamate and troleandomycin, respectively) and the NADPH-generating system (with inclusion of NADP), prior to the addition of trabectedin. Solvent control incubates were run in parallel. Incubations using boiled microsomal preparations were performed to evaluate the chemical stability of trabectedin. Incubations of unlabelled trabectedin in human liver microsomes were also performed in the presence of inhibitory antibodies raised against different human CYPs. Buffered solutions of the monoclonal antibodies were used as received from the suppliers without further dilution. Per sample, 50 μg of microsomal protein and 50 μl of monoclonal antibody were incubated. The human liver microsomes were preincubated with the antibodies for 15 min. Subsequently, the samples were incubated for 0 and 20 min under conditions identical to those described for the chemical inhibitors. Control incubates with pre-immune IgG from rabbit were run in parallel.

All enzymatic reactions in the different CYP phenotyping experiments were terminated by snapfreezing the samples in dry ice, after which they were stored at or below −18 °C until analysis.

2.5. Analytical methods

2.5.1. Radio–HPLC

Incubates of [^{14}C]trabectedin with liver subcellular fractions and with recombinant systems were analyzed by radio–HPLC. The samples were thawed in the presence of DMSO at a sample/DMSO ratio of 1:1 (v/v). The samples were sonicated and centrifuged for 10 min at 13,800 × *g* prior to HPLC analysis. For radioactivity determination, appropriate aliquots (5–50 μl) of the samples were mixed with 10 ml of Ultima Gold™ (Packard) scintillation cocktail. Liquid scintillation counting was performed using a Packard 2100 TR microprocessor controlled multi-user liquid scintillation system.

To limit chemical degradation, the radio–HPLC analysis was performed immediately after thawing the samples. The HPLC apparatus consisted of a Waters 2695 Alliance Separation Module. The samples were chromatographed on a stainless steel column (30 cm × 4.6 mm I.D.) packed with Kromasil C-18 (5 μm, Akzo Nobel). On-line radioactivity detection of HPLC eluates was carried out with a Berthold Radioactivity Monitor LB 509 system. The eluates were mixed with Ultima-Flo™ (Packard) as a scintillation cocktail delivered by a Berthold LB 5035-3 pump at a flow rate of 4.0 ml/min. UV-detection was performed at 280 nm using a Waters 996-diode array detector. Elution started with a linear gradient at a flow rate of 1 ml/min from 100% solvent system A (0.1 M ammonium acetate pH 6.25) to 100% solvent system B (water/acetonitrile, 10:90, by vol.) over 60 min followed by continued elution in the latter solvent mixture for 5 min. Injected amounts of radioactivity in the samples ranged from about 18,000 to about 61,000 dpm.

The amounts of parent drug and of its major metabolites were calculated from the radioactivity peaks following reversed-phase radio–HPLC analysis. Data processing was performed using Millennium^{32} Chromatography Software.

2.5.2. Metabolite identification

A QTOF (quadrupole time-of-flight) Ultima mass spectrometer (Waters, Millford, MA, USA) was used for metabolite identification. The mass spectrometer was equipped with a dual electrospray ionization probe and was operated in the positive ion mode at a resolution of 8000 (FWHM at *m/z* 409). The source temperature was 100 °C, desolvation temperature 250 °C and the cone voltage was set at 40 V. The second LockSpray™ ESI probe provided an

independent source of the lock mass calibrant $H_3PO_4{\cdot}NH_4^+$. The cluster ion at m/z 409.94184 was used as the calibrant in full MS, whereas the ion at m/z 392.91534 (daughter ion of m/z 490.9) was used as the lock mass in MS/MS mode. Data were acquired in the centroid mode with a scantime of 1 s and processed using Masslynx v. 4.0 software. The same chromatographic conditions were used as for the radio–HPLC analyses.

In addition to metabolite identification by LC–MS/MS, metabolite characterization was also performed by comparison of the radio–HPLC chromatograms with HPLC chromatograms of unlabelled authentic compounds. For this purpose, a mixture of the parent drug and of various authentic substances was co-chromatographed with the radioactive samples on the reversed-phase column. The authentic substances were detected by UV-monitoring at 280 nm, the metabolites by radioactivity monitoring.

2.5.3. Quantification of trabectedin (CYP phenotyping experiments with chemical inhibitors and inhibitory antibodies)

The concentration of trabectedin in the incubates of human liver microsomes with CYP-specific chemical inhibitors and inhibitory antibodies was determined by LC–MS/MS. Hundred-microliter aliquots of the incubates were spiked with 10 ng of the stable isotope labelled internal standard (tri-deuterated trabectedin) and 250 μl of methanol was added. After vortex mixing and centrifugation, the supernatants were transferred to an injection vial and mixed with 400 μl of water. The supernatants were analyzed using column switching, coupled to tandem mass spectrometry for detection. Fifty-microliter aliquots of the supernatants were injected on a trapping column (10 mm × 2.1 mm I.D., packed with 3.5 μm Symmetry Shield RP). The loading mobile phase was a water/methanol mixture (95/5; v/v) pumped at 0.5 ml/min. After loading the samples, the column was washed by increasing the methanol content to 50%. After 3 min, the trapping column was back-flushed with a water/methanol mixture (5/95; v/v) at a flow rate of 0.5 ml/min and the analyte and its internal standard eluted onto the analytical column (30 mm × 2.1 mm ID; packed with 3 μm Atlantis Hilic silica) connected to the mass spectrometer (triple quadrupole API 4000). Ionization was by turbo ion spray, operated in the positive mode. Trabectedin and its internal standard were monitored at mass transitions m/z 744.3 → 495 and 747.3 → 496, respectively.

2.6. Data analysis

For metabolite profiling, the relative amounts of unchanged trabectedin and of its major metabolites were expressed as the percentage of radioactivity in the samples accounted for by the individual radiolabelled compounds. Qualitative as well as quantitative comparisons between man and monkey were made. In the experiments with recombinant systems for CYP phenotyping, only the disappearance of parent drug and concurrent appearance of additional radioactive peaks in the radiochromatograms were considered. In the experiments with diagnostic inhibitors and with CYP inhibitory antibodies, the concentration of trabectedin in the incubation mixtures with and without inhibitors as a function of incubation time was calculated.

3. Results

3.1. Metabolite profiles

[^{14}C]trabectedin (5 μM) was incubated for 120 min with 12,000 × g liver supernatant fractions of male Cynomolgus monkeys and man. The metabolite profiles of trabectedin in the incubates of both species were defined by radio–HPLC (Fig. 2).

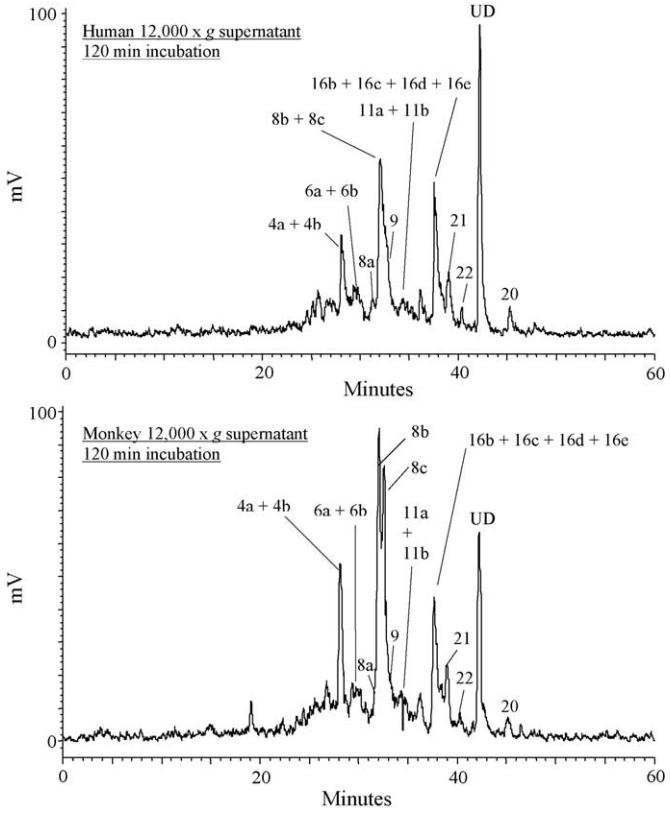

Fig. 2. Radio–HPLC chromatograms of [^{14}C]trabectedin (5 μM) with human (top chromatogram) and Cynomolgus monkey (bottom chromatogram) hepatic 12,000 × g supernatant fractions following a 2-h incubation. Radiolabelled compounds are coded as described in the Section 3.

Metabolite designation was based on their retention time in the radio–HPLC chromatograms. As several radioactivity peaks were composed of two or more co-eluting metabolites under the HPLC conditions used, a suffix (letter) was added to identify individual metabolites. The radio–HPLC chromatograms indicate that liver subcellular fractions of the Cynomolgus monkey and of human produced a similar pattern of radiolabelled metabolites, although some quantitative differences were noticeable. Four major chromatographic peaks were observed with retention times of about 28, 32, 37 and 42 min. Unchanged trabectedin accounted for 14.9% and 9.2% of the injected sample radioactivity in liver subcellular fractions of human and Cynomolgus monkey, respectively, indicating that the metabolism of trabectedin proceeded faster in monkeys than in humans. Due to incomplete radio–HPLC separation, the abundance of individual metabolites in the major peaks could not be determined. Relative amounts of co-eluting metabolites are given in Table 1. Visual inspection of the metabolite profiles in Fig. 2 revealed a higher abundance of the 4a/4b and 8b/8c metabolites in monkey fractions than in human fractions, suggesting a more active biotransformation of trabectedin via *N*-demethylation (metabolite 8b) and/or via demethylation with additional mono-oxidation (metabolite 4b), di-oxidation (metabolite 4a) or tri-oxidation (metabolite 8c) in monkeys than in humans. LC–MS/MS analysis (see below) revealed that the trabectedin metabolites identified in hepatic subcellular fractions of Cynomolgus monkey were similar to those of human.

3.2. Structure elucidation of metabolites

Trabectedin metabolites were identified by LC–MS/MS and HPLC co-chromatography using unlabelled trabectedin and

Table 1
Comparative metabolism of [^{14}C]trabectedin in hepatic 12,000 × *g* supernatant fractions of humans and Cynomolgus monkeys.

In vitro metabolic profiling in hepatic 12,000 × *g* supernatant fractions			
Metabolite		Human	Cynomolgus monkey
4a		√[b]	√
4b		√	√
	Relative amount of 4a + 4b	++	++
6a		√	√
6b		√	√
	Relative amount of 6a + 6b	+	+
8a		√	√
8b		√	√
8c		√	√
9		√	√
	Relative amount of 8a + 8b + 8c + 9	+++	+++
11a		√	√
	Relative amount of 11a + 11b[a]	+	+
16b		√	√
16c		√	√
16d		√	√
16e		√	√
	Relative amount of 16b + 16c + 16d + 16e	++	++
UD		√	√
	Relative amount of unchanged drug (trabectedin)	++	++

Relative amounts are expressed as + (1–5%), ++ (>5–15%), +++ (>15%).
[a] 11b is a chemical degradant.
[b] Detected.

authentic reference compounds. The MS spectrum of trabectedin showed a protonated molecular ion at *m*/*z* 762. Fragmentation of the parent ion produced characteristic fragment ions, useful for metabolite identification (Fig. 3). MS^2 spectra of the various metabolites are provided in Figs. 4 and 5. Because of the complexity of the molecule and the multiple potential sites for metabolism, it was generally not possible to identify the exact site of metabolic conversion based on the available LC–MS/MS data. Nonetheless, the data allowed for partial structure elucidation of the metabolites and identification of the molecular substructures undergoing metabolism.

The molecular ion fragments of the metabolites are listed in Table 2. By using a QTOF mass spectrometer, it was possible to obtain accurate masses for the pseudomolecular ions of the metabolites in MS and their product ions generated in MS^2. The accurate masses obtained were processed using the elemental composition calculator of the Masslynx software, and possible molecular formulae were calculated. All measured accurate masses were within a 5 ppm error relative to the corresponding calculated masses (Table 3). Based on the QTOF measurements, the following metabolites were identified:

3.2.1. Metabolite 4a

The mass spectrum of metabolite 4a revealed a protonated molecular ion at *m*/*z* 780, corresponding to a 18 amu shift relative to trabectedin (*m*/*z* 762). A similar 18 amu shift was noticed in the MS/MS fragmentation of specific protonated molecular ion fragments (Table 2) while the fragments at *m*/*z* 224 and 260 were unchanged. The product ions at *m*/*z* 234 and 493 are the result of water loss of fragments *m*/*z* 252 and 511, respectively. The LC–MS/MS data indicate that metabolite 4a is the result of a demethylation in combination with a double oxidation at the A domain of trabectedin.

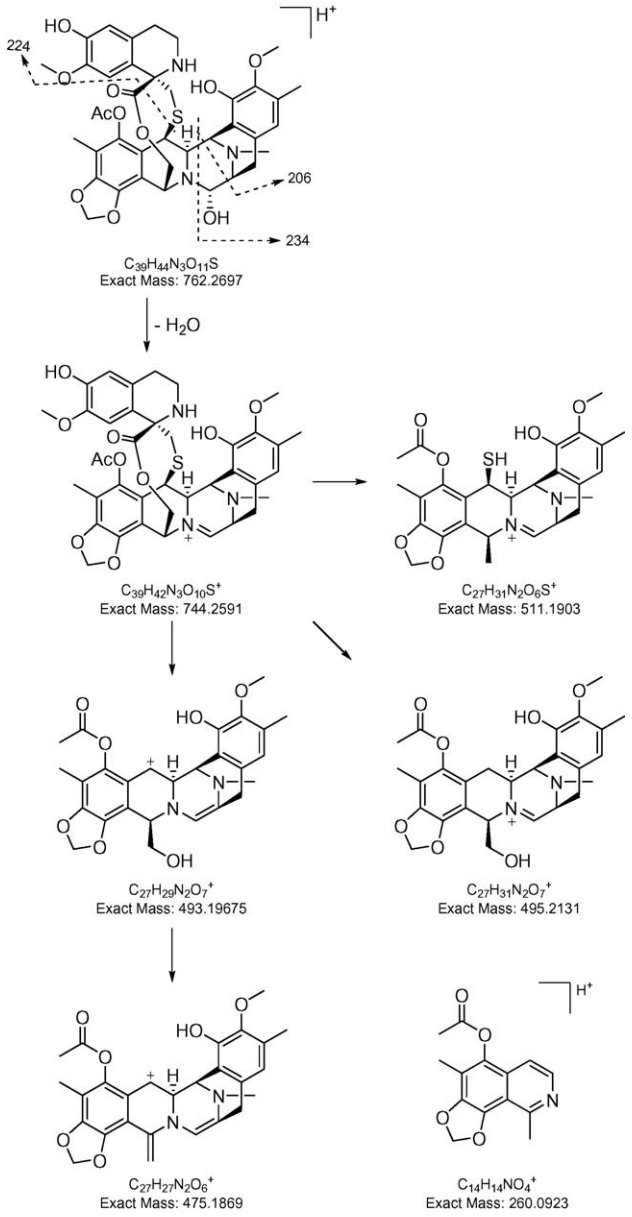

Fig. 3. Mass spectrometric fragmentation of trabectedin.

3.2.2. Metabolites 4b and 6a

The protonated molecular ions of metabolites 4b and 6a and several corresponding MS/MS product ions were shifted 2 amu (*m*/*z* 764) as compared to trabectedin (Table 2). This suggests that both metabolites are the result of a combined demethylation and oxidation reaction at the A domain of the molecule.

3.2.3. Metabolite 6b

Metabolite 6b showed the same protonated molecular ion (*m*/*z* 762) and corresponding MS/MS product ions at *m*/*z* 206, 224, 260 and 475 (Table 2) as compared to trabectedin. However, in comparison to the unchanged drug a different accurate mass was obtained (Table 3), indicating a different elemental composition. The minor water loss from the molecular ion observed in full MS and the presence of an abundant product ion at *m*/*z* 206 suggested that the hydroxyl function at the carbinolamine moiety was still intact. Taken together, these data indicate that metabolite 6b is likely the result from a demethylation and a mono-oxidation combined with a loss of two hydrogen atoms at the A domain of trabectedin.

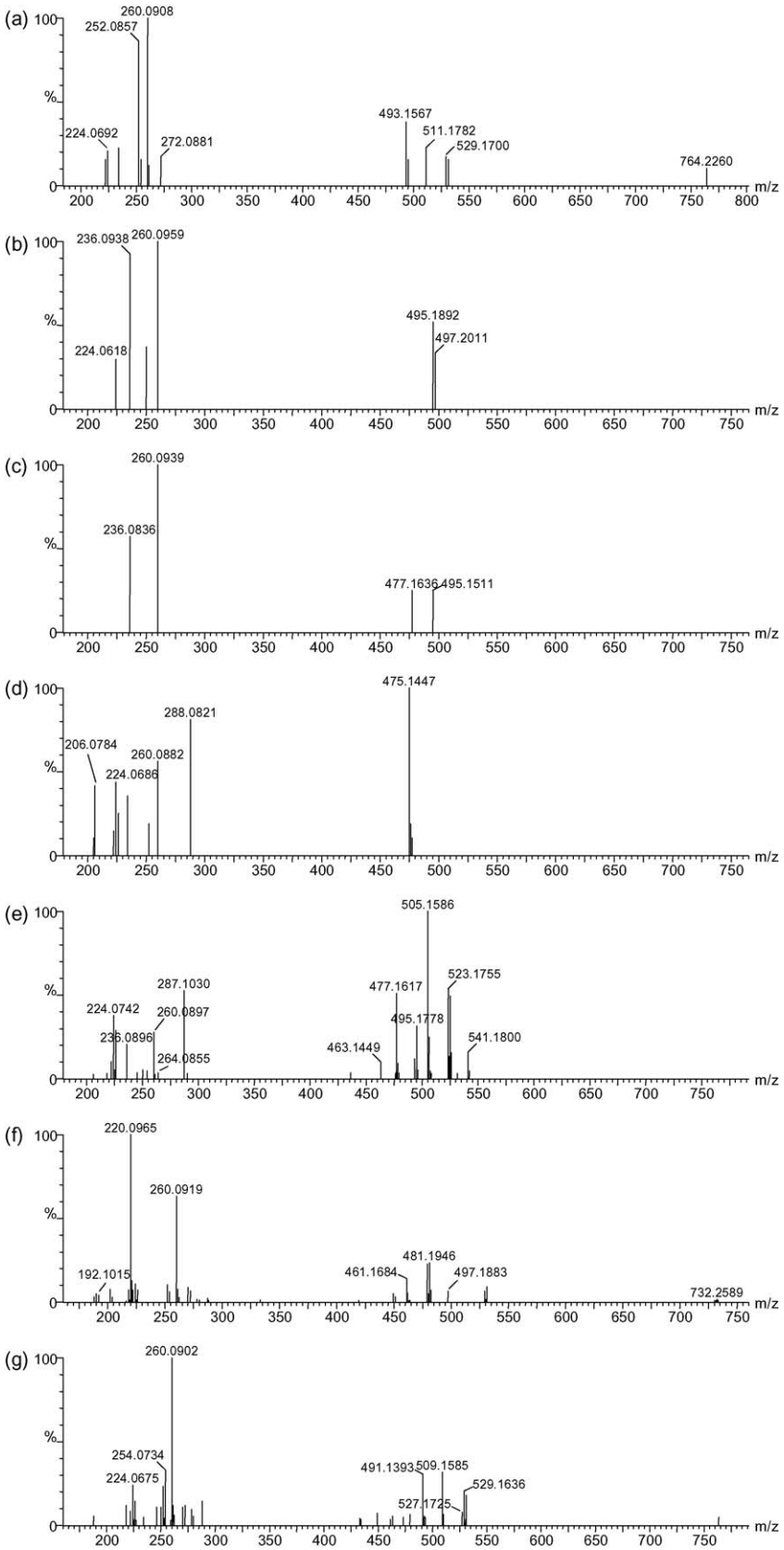

Fig. 4. MS^2 spectra of (a) metabolite 4a, (b) metabolite 4b, (c) metabolite 6a, (d) metabolite 6b, (e) metabolite 8a, (f) metabolite 8b and (g) metabolite 8c.

Table 2
Identification of trabectedin metabolites from radio–HPLC and LC–MS(MS) analyses of incubates with hepatic 12,000 × *g* supernatant fractions from human and Cynomolgus monkey.

Metabolite code	Metabolic step	Identification method	$M+H^+$	Typical MS/MS fragments (*m*/*z*)
4a	Demethylation + di-oxidation	LC–MS	780 (+18)	252 (234 + 18), 511 (493 + 18), 529 (511 + 18), 224, 260
4b	Demethylation + mono-oxidation	LC–MS	764 (+2)	236 (234 + 2), 495 (493 + 2), 497 (495 + 2), 224, 260
6a	Demethylation + mono-oxidation	LC–MS	764 (+2)	236 (234 + 2), 477 (475 + 2), 495 (493 + 2), 497 (495 + 2), 260
6b	Demethylation + mono-oxidation + loss of two hydrogen atoms	LC–MS	762	206, 224, 260, 475
8a	Carboxylic acid formation	LC–MS	792 (+30)	236 (206 + 30), 264 (234 + 30), 505 (475 + 30), 523 (493 + 30), 525 (495 + 30), 541 (511 + 30), 224, 260, 477 (523–46), 495 (541–46)
8b	*N*-demethylation	Co-chromatography (ET-729), LC–MS	748 (−14)	220 (234–14), 192 (206–14), 461 (475–14), 479 (493–14), 481 (495–14), 497 (511–14), 260
8c	Demethylation + tri-oxidation including oxidation of the carbinolamine moiety to an amide	LC–MS	778 (+16)	224, 260, 491 (475 + 16), 509 (493 + 16), 527 (511 + 16)
9	Aliphatic ring opening	LC–MS	750 (−12)	206, 234, 463 (493–12), 481 (493–12), 483 (495–12)
11a	Mono-oxidation	LC–MS	778 (+16)	222 (206 + 16), 250 (234 + 16), 491 (475 + 16), 509 (493 + 16), 511 (495 + 16), 224, 260
16b	Di-oxidation	LC–MS	794 (+32)	238 (206 + 32), 266 (234 + 32), 507 (475 + 32), 525 (493 + 32), 543 (511 + 32), 224, 260
16c	*O*-demethylation	LC–MS	748 (−14)	210 (224–10), 206, 234, 260, 475, 493, 495
16d	Demethylation + mono-oxidation + loss of two hydrogen atoms	LC–MS	762	206, 224, 260, 475, 493, 495, 511
16e	Carboxylic acid formation + mono-oxidation	LC–MS	790 (+28)	503 (475 + 28), 521 (493 + 28), 523 (495 + 28), 539 (511 + 28), 224; 493 (521–46), 475 (539–46)
UD	–	Co-chromatography (ET-743), LC–MS	762	206, 224, 234, 260, 475, 493, 495, 511, 744

3.2.4. Metabolite 8a

The protonated molecular ion of metabolite 8a had a 30 amu shift (*m*/*z* 792) relative to trabectedin. Several product ions at *m*/*z* 236, 264, 505, 523, 525 and 541 displayed a 30 amu shift as well. The loss of 46 amu from fragment ions at *m*/*z* 523 and 541, giving product ions at *m*/*z* 477 and 495, respectively, suggested carboxylic acid formation at the A domain of the molecule.

3.2.5. Metabolite 8b

The protonated molecular ion of metabolite 8b had lost 14 amu (*m*/*z* 748) relative to trabectedin. The same shift was also seen with selected product ions (Table 2) indicating a demethylation of these fragments. The fragmentation behaviour and retention time of metabolite 8b proved to be identical to that of the authentic reference compound ET-729 (*N*-demethylated trabectedin).

3.2.6. Metabolite 8c

The protonated molecular ion of metabolite 8c had a 16 amu shift (*m*/*z* 778) relative to trabectedin. The product ions at *m*/*z* 224 and 260 were unchanged, whereas the product ions at *m*/*z* 491, 509 and 527 were shifted 16 amu. The product ion at *m*/*z* 224 can be explained as 206 + 18 since the fragment at *m*/*z* 252 had also shifted 18 amu relative to *m*/*z* 234 of the parent drug. Although a shift of 16 amu may suggest a simple oxidation, this was not in accordance with the accurate mass measurements (Table 3) that indicated an elemental composition of $C_{38}H_{40}N_3O_{13}S$. The accurate mass measurements therefore suggested that metabolite 8c is likely the result of demethylation in combination with a triple oxidation, including an oxidation of the carbinolamine moiety to an amide, at the trabectedin A domain.

3.2.7. Metabolite 9

The protonated molecular ion was observed at *m*/*z* 750, or 12 amu less than the drug substance (*m*/*z* 762). This 12 amu shift was also reflected in several product ions (Table 2). Based on the elemental composition ($C_{38}H_{44}N_3O_{11}S$) inferred from the accurate mass measurements (Table 3), the proposed metabolite is thought to be the result of an aliphatic ring opening at the methylene dioxybridge at the B subunit of trabectedin.

Table 3
Chemical formulas and accurate mass measurements of trabectedin and metabolites in incubates of [^{14}C]trabectedin with hepatic 12,000 × *g* supernatant fractions of human and Cynomolgus monkey.

Metabolite	Chemical formula	$[M+H]^+_{calculated}$	$[M+H]^+_{experimental}$		$Error_{QTof}$ (ppm)	
			Human	Monkey	Human	Monkey
4a	$C_{38}H_{42}N_3O_{13}S$	780.2438	780.2432	780.2440	−0.9	0.2
4b	$C_{38}H_{42}N_3O_{12}S$	764.2489	764.2460	764.2489	−3.8	0.0
6a	$C_{38}H_{42}N_3O_{12}S$	764.2489	764.2503	764.2471	1.8	−2.4
6b	$C_{38}H_{40}N_3O_{12}S$	762.2333	762.2327	762.2329	−0.7	−0.5
8a	$C_{39}H_{42}N_3O_{13}S$	792.2438	792.2449	792.2477	1.4	4.9
8b	$C_{38}H_{42}N_3O_{11}S$	748.2540	748.2549	748.2531	1.3	−1.2
8c	$C_{38}H_{40}N_3O_{13}S$	778.2282	778.2319	778.2266	4.8	−2.1
9	$C_{38}H_{44}N_3O_{11}S$	750.2697	750.2672	750.2670	−2.4	−3.6
11a	$C_{39}H_{44}N_3O_{12}S$	778.2646	778.2656	778.2625	1.4	−2.7
16b	$C_{39}H_{44}N_3O_{13}S$	794.2595	794.2618	794.2625	3.0	3.8
16c	$C_{38}H_{42}N_3O_{11}S$	748.2540	748.2541	748.2551	0.2	1.5
16d	$C_{38}H_{40}N_3O_{12}S$	762.2333	762.2343	762.2346	1.3	1.7
16e	$C_{39}H_{40}N_3O_{13}S$	790.2282	790.2296	790.2289	1.8	0.9
Unchanged drug (trabectedin)	$C_{39}H_{44}N_3O_{11}S$	762.2697	762.2705	762.2700	1.1	0.4

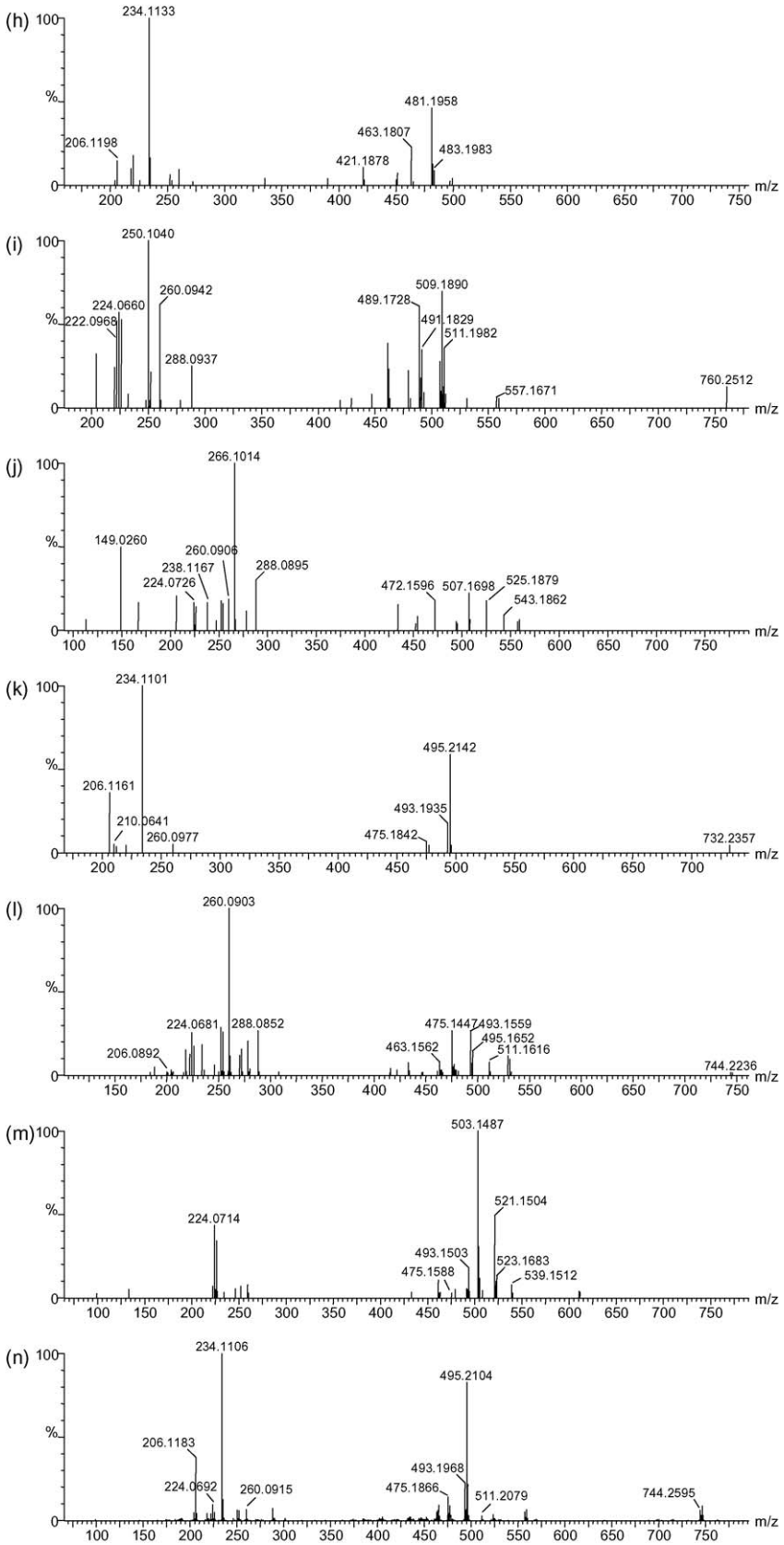

Fig. 5. MS^2 spectra of (h) metabolite 9, (i) metabolite 11a, (j) metabolite 16b, (k) metabolite 16c, (l) metabolite 16d, (m) metabolite 16e and (n) unchanged drug (trabectedin).

3.2.8. Metabolite 11a

The protonated molecular ion of metabolite 11a (*m*/*z* 778) and several product ions at *m*/*z* 222, 250, 491, 509 and 511 were shifted 16 amu as compared to unchanged drug (Table 2), while the fragment ions at *m*/*z* 224 and 260 were unchanged. These data indicate that metabolite 11a results from a mono-oxidation at the A subunit of trabectedin.

3.2.9. Metabolite 16b

The protonated molecular ion of metabolite 16b (*m*/*z* 794) and several product ions at *m*/*z* 238, 266, 507, 525 and 543 were shifted 32 amu as compared to trabectedin (Table 2), while the fragment ions at *m*/*z* 224 and 260 were unchanged. Collectively, these data indicate that metabolite 16b is the result of a double oxidation at the A domain of trabectedin.

3.2.10. Metabolite 16c

The protonated molecular ion of metabolite 16c had lost 14 amu (*m*/*z* 748) relative to trabectedin. The same 14 amu shift was observed for the small fragment peak (Fig. 5) at *m*/*z* 210. All other product ions were identical to those detected for the unchanged drug (Table 2). Metabolite 16c is therefore considered to be the result of a *O*-demethylation reaction at the C domain of trabectedin.

3.2.11. Metabolite 16d

Metabolite 16d showed the same protonated molecular ion (*m*/*z* 762) and corresponding MS/MS product ions at *m*/*z* 206, 224, 260, 475, 493, 495 and 511 (Table 2) as compared to trabectedin. However, in comparison with unchanged drug, a different accurate mass was observed (Table 3), indicating a different elemental composition. The abundant water loss from the molecular ion, seen in full MS and MS/MS, and the presence of a small product ion at *m*/*z* 206, suggested that the hydroxyl function at the carbinolamine moiety was still intact. Metabolite 16d is therefore thought to be the result of a demethylation and a mono-oxidation in combination with a loss of two hydrogen atoms at the trabectedin A domain.

3.2.12. Metabolite 16e

The protonated molecular ion of metabolite 16e (*m*/*z* 790) and several product ions at *m*/*z* 503, 521, 523 and 539 (Table 2) were shifted 28 amu as compared to trabectedin. A loss of 46 amu (–HCOOH) from the product ions at *m*/*z* 521 and 539, giving product ions at *m*/*z* 475 and 493, respectively, and the absence of a water loss from the molecular ion suggesting the absence of the hydroxyl function at the carbinolamine moiety. This indicated that metabolite 16e results from carboxylic acid formation in combination with a mono-oxidation at the A subunit of trabectedin.

A proposed metabolic scheme of trabectedin based on the *in vitro* metabolic data for monkey and man is presented in Fig. 6. Trabectedin was metabolized via different biotransformation pathways including *N*-demethylation, *O*-demethylation, carboxylic acid formation (alone or in combination with oxidation), mono- and di-oxidation, aliphatic ring opening, and demethylation in combination with mono-, di- or tri-oxidation. Most of the metabolic conversions occurred at the trabectedin A domain including mono-oxidation (metabolite 11a) and di-oxidation (metabolite 16b), carboxylic acid formation with and without additional oxidation (metabolites 16e and 8a, respectively), and demethylation either without (metabolite 8b, ET-729) or with additional mono-oxidation (metabolites 4b and 6a), di-oxidation (metabolites 4a, 16d and 6b) or tri-oxidation (metabolite 8c). Only two metabolic conversions were detected at the B and C domains of trabectedin, viz. aliphatic ring opening of the methylene dioxybridge at the B domain (metabolite 9) and *O*-demethylation at the C subunit (metabolite 16c). Overall, demethylation and oxidation played a major role in phase I metabolism of the drug. All biotransformation pathways were observed in liver subcellular fractions of both the Cynomolgus monkey and human.

Besides these metabolic products, LC–MS/MS analysis revealed the presence of traces of four cyano compounds in incubations with both monkey and human 12,000 × *g* liver supernatants. The occurrence of these compounds (coded 11b, 20, 21 and 22) in the incubates can hardly be explained by metabolism. They are considered to be degradation products rather than genuine metabolites. Their presence is probably due to cyano impurities in the [^{14}C]trabectedin batch. Compound 20, the cyano derivative of unchanged trabectedin, was observed in incubates with boiled liver subcellular fractions. The other compounds might be formed chemically as cyano derivatives of biotransformation products after demethylation and/or aliphatic ring opening.

Upon incubation of [^{14}C]trabectedin with monkey and human liver microsomes in the presence of UDPGA, two peaks corresponding to unchanged drug substance and the degradation compound 20, were predominantly present in radio–HPLC chromatograms of both boiled and non-boiled samples. Two additional minor peaks were present in non-boiled samples of both human and monkey liver microsomes, constituting 4% of the injected radioactivity at the most (data not shown). These results indicate that trabectedin is not substantially metabolized via glucuronidation *in vitro*. However, the incubations with liver microsomes in the presence of UDPGA did not allow one to assess possible glucuronidation of phase I metabolites of trabectedin. Conversely, the omission of UDPGA in incubates with 12,000 × *g* supernatants in the presence of a NADPH-generating system likely prevented oxidative metabolites from undergoing subsequent glucuronidation.

3.3. CYP phenotyping

[^{14}C]trabectedin (5 μM) was incubated for 120 min with *E. coli* membranes, which stably express single human CYP isozymes together with NADPH-P450 reductase. Incubation with heterologously expressed CYP1A2, 2A6, 2B6, 2C8, 2C9, 2C18, 2D6, 2E1, 3A4 and 3A5 resulted in disappearance of the parent compound and concurrent formation of radiolabelled metabolites. In contrast, CYP1B1, 2C19, and 4A11 did not metabolize the drug to a notable extent (data not shown).

To further delineate the involvement of specific CYP isoforms in the metabolism of trabectedin, separate inhibition experiments were performed at a clinically relevant trabectedin drug level. To that aim, the effect of chemical and immunoinhibition on the disappearance of trabectedin was investigated in pooled human liver microsomes at a trabectedin concentration of 10 ng/ml (13 nM). In Fig. 7, the disappearance of trabectedin from the incubation mixture as a function of incubation time is presented in the absence and in the presence of CYP-isoform selective chemical inhibitors and inhibitory antibodies. The results from these experiments showed that the disappearance of trabectedin from the incubation mixture was virtually completely inhibited by selective chemical CYP3A4 inhibitors (ketoconazole and troleandomycin) as well as by selective inhibitory antibodies directed against CYP3A4.

4. Discussion

Available data indicate that trabectedin is extensively metabolized in humans and that its oxidative metabolism is very complex, resulting in a large number of metabolites [8]. Despite the longstanding clinical use of the compound, its

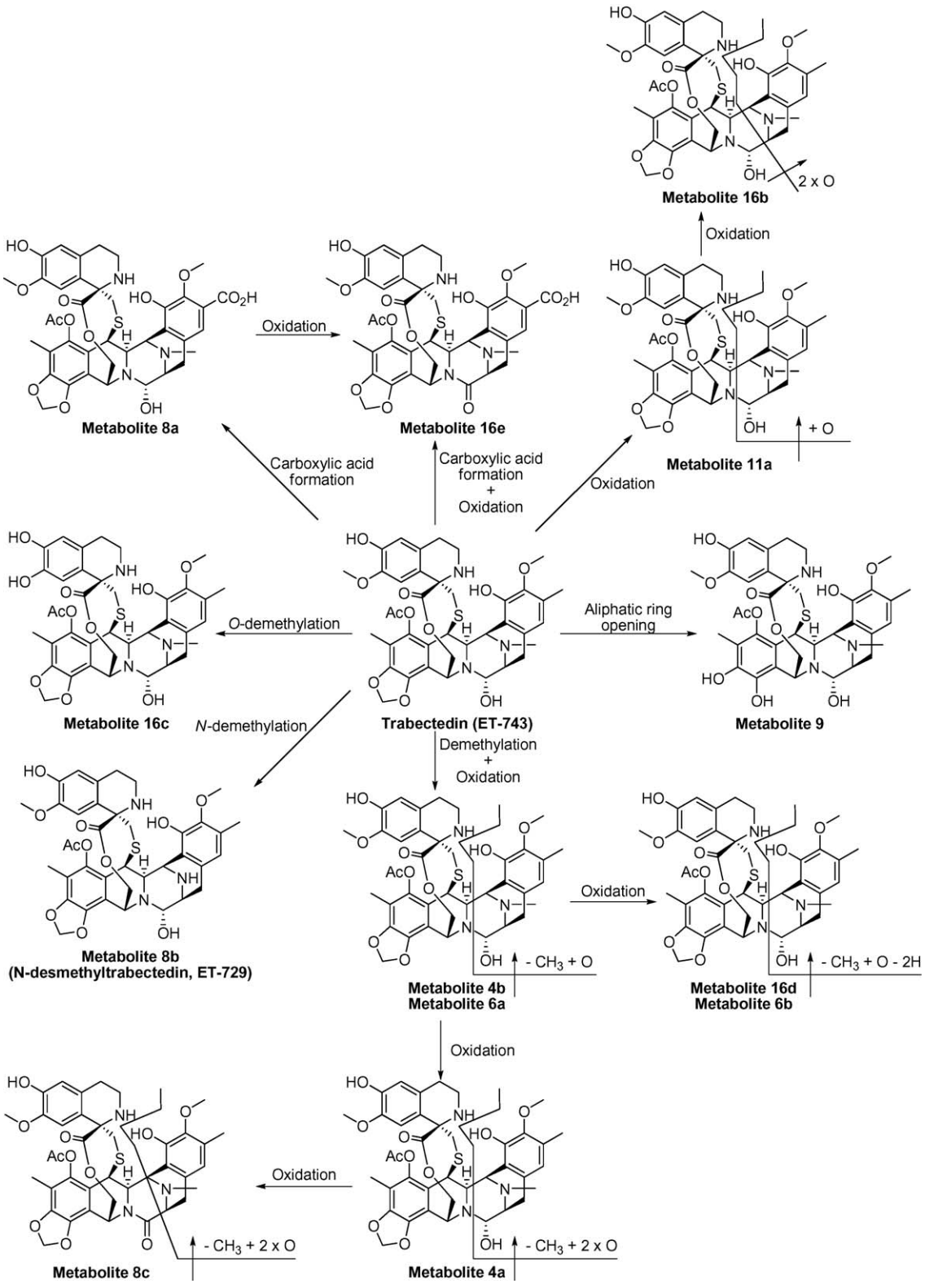

Fig. 6. Proposed *in vitro* metabolic pathways of trabectedin in hepatic 12,000 × *g* supernatant fractions of the Cynomolgus monkey and human.

metabolism has not been well defined. *In vivo* investigations have been especially difficult because of several compound related factors including the low dose, the extent and complexity of metabolism, the extremely low metabolite concentrations, low faecal extraction recoveries, and stability issues with trabectedin and some of its metabolites [5,7,8]. Owing to these complicating factors, literature data on the identification of trabectedin metabolites are scarce. Sparidans et al. [5] identified a few metabolites and degradation products in *in vitro* incubates with human liver microsomes and plasma, but attempts to detect these metabolites in patient samples were unsuccessful. Reid et al. [6] investigated the metabolism of trabectedin in rat and human liver microsomes, and in cDNA-expressed human CYP enzymes. The authors identified three oxidative metabolites in cDNA-expressed

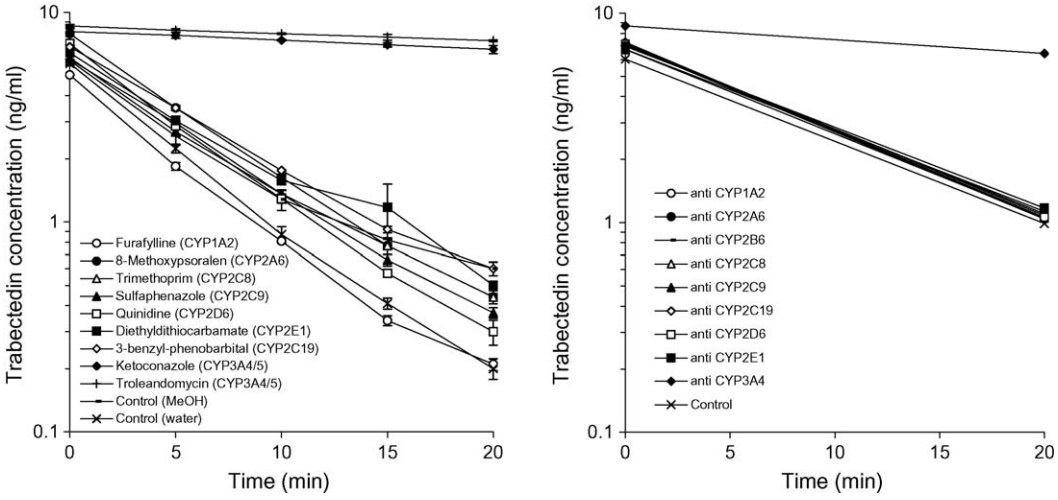

Fig. 7. Effect of various CYP isoform-selective inhibitors (left panel: chemical inhibitors; right panel: inhibitory monoclonal antibodies) on the depletion of trabectedin (13 nM; 10 ng/ml) in pooled human liver microsomes. The CYP isoform(s) specifically inhibited by the chemical inhibitors are indicated between brackets. Each data point represents the mean of three (experiments with chemical inhibitors) or two determinations (experiments with inhibitory antibodies).

CYP systems, namely a metabolite with the intact trabectedin B subunit ($C_{15}H_{16}NO_6$; $[M+H]^+$ at m/z 306.0977), a metabolite containing an *N*-methylisoquinolinium skeleton ($C_{12}H_{14}NO_2$; $[M+H]^+$ at m/z 204.1024) and the *N*-demethylated metabolite ET-729. Recently, Beumer et al. [8] reported on *in vivo* metabolite profiling work obtained from a clinical mass balance study with [^{14}C]trabectedin in cancer patients. Radio–HPLC analysis of urine and faeces samples indicated the formation of a large number of trabectedin metabolites. However, the structure of only a few putative trabectedin metabolites (ET-745, ET-759A, ETM-259, ETM-217, and ET-204) was tentatively identified [8].

Vermeir et al. [9] investigated the *in vitro* metabolism of trabectedin in hepatic subcellular fractions of various species including humans. Data from that study suggested similarity in trabectedin's hepatic metabolism between Cynomolgus monkeys and humans, while that of other species including rat and dog were quite different. However, the data from that study were considered suboptimal and inconclusive in a sense that the identification of some metabolites was mainly based on co-chromatography with authentic reference compounds, leaving the majority of the biotransformation products unidentified.

To facilitate the identification of the major metabolites, several parameters were optimized in the current *in vitro* study, including the selection of the substrate concentration (5 μM instead of 1.6 μM) and the use of a highly sensitive QTOF Ultima mass spectrometer. In addition, the risk for degradation of trabectedin and/or its metabolites was minimized by immediate injection of the samples after thawing.

In the present work, the structure of major human and monkey *in vitro* metabolites was elucidated. Identified metabolites mainly resulted from biotransformations at the trabectedin A domain and included mono-oxidation and di-oxidation, carboxylic acid formation with and without additional oxidation, and demethylation either without (*N*-demethylation to ET-729) or with additional mono-, di- or tri-oxidation. Only two metabolic conversions were detected at the B and C domains of trabectedin, viz. aliphatic ring opening of the methylene dioxybridge at the B domain and *O*-demethylation at the C subunit. Individual LC–MS/MS analyses of human and monkey samples showed that all metabolites identified in human liver fractions were also present in those of the Cynomolgus monkey. Radio–HPLC analysis showed that trabectedin's metabolism is faster in monkeys than in humans. In addition, trabectedin proved to be more actively metabolized via *N*-demethylation and/or via demethylation with additional mono-, di- or tri-oxidation in monkeys than in humans.

With the exception of ET-729, none of the proposed *in vivo* trabectedin metabolites identified by Beumer et al. [8] were detected in the current *in vitro* study. This may be explained by several limitations of the *in vivo* metabolite profiling study. In the latter study, only metabolite fragments from available reference compounds were monitored in the *in vivo* samples by LC–MS/MS, which precluded the detection of trabectedin's oxidized metabolites, as identified in the current *in vitro* study. In addition, the low extraction efficiency (about 30%) from the faeces, i.e. the major route of excretion, and the instability of metabolites during sample workup may also have contributed to the apparent discrepancy between the current *in vitro* and previously published *in vivo* metabolite profiling data.

In patient samples, ET-729 was detected as a potential metabolite in faeces extracts, but ET-729 was also identified as chemical degradant [8]. LC–MS analysis of *in vivo* samples from trabectedin-treated patients did not result in the detection of ET-729 [5]. The present *in vitro* work showed that formation of this metabolite through *N*-demethylation is a genuine metabolic conversion.

In the *in vivo* metabolite profiling work of Beumer et al. [8], several ETM-coded compounds resulting from breaking up of the trabectedin molecule to its individual tetrahydroisoquinoline subunits have been proposed as possible trabectedin metabolites. These compounds were not detected in the present *in vitro* work. Formation of this kind of compounds via metabolic conversion is not very likely and it has not been described for any structurally related compound. It is conceivable that they are in fact artefacts resulting from fragmentation of trabectedin and/or its metabolites in the source of the mass spectrometer. Both the dehydroxylated metabolite ET-745 and its corresponding *N*-dealkylated metabolite ET-731 were detected in the faeces of patients, but not in the current *in vitro* study. Beumer et al. [8] argued that the unusual dehydroxylation reaction probably occurs through the activity of intestinal bacterial flora.

Possible glucuronidation of trabectedin was studied in a separate set of experiments. Because of the experimental design, possible glucuronidation of phase I metabolites of trabectedin could not be evaluated. The results suggested that trabectedin may be glucuronidated, albeit to a limited extent. Brandon et al. [17] have published similar findings, and additionally demonstrated

conjugation by glutathione-*S*-transferase, but not by sulfotransferase. Although the kinetics of trabectedin UGT-mediated glucuronidation have not been studied, the *in vivo* relevance of this pathway is questionable given the generally low affinity of UGT substrates towards these enzymes [27,28]. This may also hold true for glutathione-S-transferase mediated conjugation as the amount of substrate consumed was limited [17].

From both a drug development and a regulatory perspective, metabolism data are important as they can be used to support the selection of animal species for toxicity testing and to support/explain clinical findings [29]. Such data are considered particularly relevant to trabectedin, which has been shown to increase various markers of hepatotoxicity in all species, but with marked interspecies differences [7]. Previous *in vitro* metabolism data [9] suggested similarity in trabectedin's hepatic metabolism between Cynomolgus monkeys and humans. The *in vitro* metabolism data in the present study, together with the comparable *in vivo* toxicological profiles [30,31], provided further supporting evidence in favour of the use of the Cynomolgus monkey as relevant and predictive animal species to evaluate human trabectedin toxicity.

The involvement of CYP in the human hepatic metabolism of trabectedin has previously been studied by several investigators [6,17]. Reid et al. [6] incubated trabectedin (50 μM or 38.1 μg/ml) together with individually cDNA expressed human CYP enzymes. Quantification of remaining trabectedin in the incubates, showed that trabectedin was metabolized by CYP3A4 and to a much lesser extent by CYPs 2C9, 2D6, and 2E1, whereas no notable metabolism by CYPs 1A1, 1A2, 2A6, 2B6, 2C8, and 2C19 was observed.

Brandon et al. [17] performed several *in vitro* investigations on the human biotransformation and CYP reaction phenotyping of trabectedin (50 μg/ml or 66 μM) in pooled human liver microsomes and CYP supersomes. Trabectedin was significantly metabolized in CYP2C9, 2C19, 2D6, 2E1 and 3A4 supersomes [17]. In addition, they determined enzyme kinetic parameters for the overall metabolism of trabectedin in pooled human liver microsomes and CYP supersomes, and estimated the relative contributions of individual CYPs from these data. However, with exception of CYP3A4 and CYP2C9 supersomes, the calculated K_m–values for the depletion of trabectedin were not comprised by the tested concentration range, impacting the reliability of the determined enzyme kinetic parameters, and the estimation of the contribution of individual CYPs.

The present studies were aimed at further defining the involvement of CYP in the hepatic metabolism of trabectedin. In a first set of experiments, in which [^{14}C]trabectedin (5 μM or 3.81 μg/ml) was incubated with heterologously expressed human CYPs, depletion of the parent compound and concomitant formation of radiolabelled metabolites was observed after incubation with CYPs 1A2, 2A6, 2B6, 2C8, 2C9, 2C18, 2D6, 2E1, 3A4 and 3A5. Virtually no metabolite formation was seen with CYP1B1, 2C19, and 4A11. In the latter experiments a supra-therapeutic concentration of trabectedin was used to allow the detection of newly formed radiolabelled metabolites.

To determine the CYP isoform(s) involved at clinically relevant concentrations of trabectedin (ng/ml range), a second set of experiments was performed. In these experiments, a substrate depletion approach was adopted since it was technically not feasible to monitor the formation of the various trabectedin metabolites at low ng/ml substrate concentrations. A sensitive LC–MS/MS method was used to monitor the temporal depletion of a therapeutically relevant trabectedin concentration (10 ng/ml) from the incubation mixture. Selective chemical inhibitors and inhibitory antibodies were used as diagnostic tools. Results from these experiments showed that trabectedin metabolism was completely abrogated by selective chemical CYP3A4 inhibitors (ketoconazole and troleandomycin) as well as selective inhibitory antibodies directed against CYP3A4. This suggests that CYP3A4 is the predominant isoform implicated in the hepatic metabolism of trabectedin at therapeutically achievable concentrations.

Brandon et al. [32] suggested that in addition to CYP3A4, trabectedin concentrations in patients may also be increased through inhibition of CYP2C9, 2C19, 2D6, and 2E1. The authors based their conclusions on *in vitro* cytotoxicity measurements of trabectedin in HepG2 cells in the presence and in the absence of metabolic inhibitors and inducers. However, the use of HepG2 cells to study *in vitro* metabolism-based drug–drug interactions is inappropriate since this cell line is known to express extremely low levels of drug metabolizing enzymes, making it unsuitable for such investigations [33,34]. In addition, the choice and concentration of the employed chemical inhibitors or inducers as diagnostic tools, was not optimal in most cases [13].

In conclusion, data from the current studies confirmed that the metabolism of [^{14}C]trabectedin is qualitatively similar in liver subcellular fractions of the Cynomolgus monkey and human. Notably, all human hepatic trabectedin metabolites are also produced by the Cynomolgus monkey, supporting the use of the Cynomolgus monkey as relevant animal model for the safety assessment of trabectedin in cancer patients. Most of the metabolites result from biotransformations at the trabectedin A subunit, and demethylation and oxidation prove to be major metabolic conversions. Data from CYP phenotyping experiments demonstrated that virtually all major CYPs are able to metabolize trabectedin, but that CYP3A4 is the main human CYP isoform at clinically achievable levels. In the absence of clinical drug–drug interaction data, caution needs to be exerted when potent CYP3A4 inhibitors or inducers are added to an existing trabectedin regimen.

Acknowledgements

The authors are grateful to Dr. Cor Janssen, Dr. Tom Verhaeghe, Bjorn Verreet and Luc Diels, BA/DMPK department of J&JPRD, for technical assistance, and to Mieke Roels for administrative help.

References

[1] D'Incalci M, Jimeno J. Preclinical and clinical results with the natural marine product ET-743. Expert Opin Investig Drugs 2003;12:1843–53.
[2] Zelek L, Yovine A, Brain E, Turpin F, Taamma A, Riofrio M, et al. A phase II study of YONDELIS® (trabectedin, ET-743) as a 24-h continuous intravenous infusion in pretreated advanced breast cancer. Br J Cancer 2006;94:1610–4.
[3] Fayette J, Coquard IR, Alberti L, Boyle H, Meeus P, Decouvelaere AV, et al. ET-743: a novel agent with activity in soft-tissue sarcomas. Curr Opin Oncol 2006;18:347–53.
[4] Carter NJ, Keam SJ, Trabectedin. A review of its use in the management of soft tissue sarcoma and ovarian carcinoma. Drugs 2007;67:2257–76.
[5] Sparidans RW, Rosing H, Hillebrand MJ, Lopez-Lazaro L, Jimeno JM, Manzanares I, et al. Search for metabolites of ecteinascidin 743, a novel, marine-derived, anti-cancer agent, in man. Anticancer Drugs 2001;12:653–66.
[6] Reid JM, Kuffel MJ, Ruben SL, Morales JJ, Rinehart KL, Squillace DP, et al. Rat and human liver cytochrome P-450 Isoform Metabolism of Ecteinascidin 743 does not predict gender-dependent toxicity in humans. Clin Cancer Res 2002;8:2952–62.
[7] Beumer JH, Schellens JHM, Beijnen JH. Hepatotoxicity and metabolism of trabectedin: a literature review. Pharmacol Res 2005;51:391–8.
[8] Beumer JH, Rademaker-Lakhai JM, Rosing H, Hillebrand MJ, Bosch TM, Lopez-Lazaro L, et al. Metabolism of trabectedin (ET-743, YONDELIS®) in patients with advanced cancer. Cancer Chemother Pharmacol 2007;59:825–37.
[9] Vermeir M, Hendrickx J, Hurkmans R, Van Houdt J, Zwijsen C, Bode W, et al. An interspecies comparison of the metabolism of the anticancer agent YONDELIS® (Trabectedin, ET-743). In: Anzenbacher P, Hudecek J, editors. Cytochromes P450, biochemistry, biophysics and drug metabolism, proceedings of the 13th international conference on cytochromes P450, Prague, Czech Republic, June 29–July 3 2003. Bologna: Monduzzi Editore; 2003. p. 327–31.
[10] Food and Drug Administration Draft Guidance for Industry. Safety testing of drug metabolites. Bethesda, MD: Center for Drug Evaluation and Research (CDER), Food and Drug Administration; 2005.
[11] Davis-Bruno KL, Atrakchi A. A regulatory perspective on issues and approaches in characterizing human metabolites. Chem Res Toxicol 2006;19:1561–3.

[12] Bjornsson TD, Callaghan JT, Einolf HJ, Fischer V, Gan L, Grimm S, et al. The conduct of *in vitro* and *in vivo* drug–drug interaction studies: a Pharmaceutical Research and Manufacturers of America (PhRMA) Perspective. Drug Metab Dispos 2003;31:815–32.
[13] Food and Drug Administration Draft Guidance for Industry. Drug interaction studies—study design, data analysis, and implications for dosing and labeling. Bethesda, MD: Center for Drug Evaluation and Research (CDER), Food and Drug Administration; 2006.
[14] Beijnen JH, Schellens JH. Drug interactions in oncology. Lancet Oncol 2004;5:489–96.
[15] Blower P, de Wit R, Goodin S, Aapro M. Drug–drug interactions in oncology: why are they important and can they be minimized? Crit Rev Oncol Hematol 2005;55:117–42.
[16] Riechelmann RP, Moreira F, Smaletz O, Saad ED. Potential for drug interactions in hospitalized cancer patients. Cancer Chemother Pharmacol 2005;56: 286–90.
[17] Brandon EF, Sparidans RW, Guijt KJ, Löwenthal S, Meijerman I, Beijnen JH, et al. *In vitro* characterization of the human biotransformation and CYP reaction phenotype of ET-743 (YONDELIS®, Trabectedin), a novel marine anti-cancer drug. Invest New Drugs 2006;24:3–14.
[18] Gillam EMJ, Baba T, Kim BR, Ohmori S, Guengerich FP. Expression of modified human cytochrome P450 3A4 in *Escherichia coli* and purification and reconstitution of the enzyme. Arch Biochem Biophys 1993;305: 123–31.
[19] Blake JAR, Pritchard M, Ding S, Smith GCM, Burchell B, Wolf CR, et al. Coexpression of a human P450 (CYP3A4) and P450 reductase generates a highly functional monooxygenase system in *Escherichia coli*. FEBS Lett 1996; 397:210–4.
[20] Guengerich FP, Martin MV, Guo Z, Chun YJ. Purification of functional recombinant P450 s from bacteria. Methods Enzymol 1996;272:35–44.
[21] Pritchard MP, McLaughlin L, Friedberg T. Establishment of functional human cytochrome P450 monooxygenase systems in *Escherichia coli*. Methods Mol Biol 2006;320:19–29.
[22] Amar-Costesec A, Beaufay H, Wibo M, Thines-Sempoux D, Feytmans E, Robbi M, et al. Analytical study of microsomes and isolated subcellular membranes from rat liver. II. Preparation and composition of the microsomal fraction. J Cell Biol 1974;61:201–12.
[23] Wang P, Mason PS, Guengerich FP. Purification of human liver cytochrome P-450 and comparison to the enzyme isolated from rat liver. Arch Biochem Biophys 1980;199:206–19.
[24] Lowry OH, Rosenbrough NJ, Farr AL, Randall RJ. Protein measurement with the folin phenol reagent. J Biol Chem 1951;193:265–75.
[25] Omura T, Sato R. The carbon monoxide-binding pigment of liver microsomes. I. Evidence for its hemoprotein nature. J Biol Chem 1964;239:2370–8.
[26] Suzuki H, Kneller MB, Haining RL, Trager WF, Rettie AE. (+)-*N*-3-benzylnirvanol and (−)-*N*-3-benzylphenobarbital: new potent and selective *in vitro* inhibitors of CYP2C19. Drug Metab Dispos 2002;30:235–9.
[27] Williams JA, Hyland R, Jones BC, Smith DA, Hurst S, Goosen TC, et al. Drug–drug interactions for UDP-glucuronosyltransferase substrates: a pharmacokinetic explanation for typically observed low exposure (AUCi/AUC) ratios. Drug Metab Dispos 2004;32:1201–8.
[28] Kiang TK, Ensom HHH, Chang TKH. UDP glucuronosyltransferases and clinical drug–drug interactions. Pharmacol Ther 2005;106:97–132.
[29] Lin JH, Lu AYH. Role of pharmacokinetics and metabolism in drug discovery and development. Pharmacol Rev 1997;49:403–49.
[30] Verbeeck J, Vynckier A, Looszova A, Anciaux K, Bode N, De Coster R, et al. Hepatotoxicological differences with ET-743 between Sprague Dawley rats and Cynomolgus monkeys.In: Proceedings of the 41st Congress of the European Society of Toxicology, Florence, Italy, September 28–October 1, 2003. Toxicol Lett 2003;144:S98.
[31] Vynckier A, De Coster R, Verbeeck J, Looszova A, Anciaux K, Verhaeghe T, et al. Hepatotoxicological differences with ET-743 in Sprague–Dawley rats and Cynomolgus monkeys. Toxicol Pathol 2005;33:P12.
[32] Brandon EF, Meijerman I, Klijn JS, den Arend D, Sparidans RW, Lazaro LL, et al. In-vitro cytotoxicity of ET-743 (Trabectedin, YONDELIS®), a marine anticancer drug, in the Hep G2 cell line: influence of cytochrome P450 and phase II inhibition, and cytochrome P450 induction. Anti-Cancer Drugs 2005; 16:935–43.
[33] Brandon E, Raap C, Meijerman I, Beijen CJ, Schellen J. An update on *in vitro* test methods in human hepatic drug biotransformation research: pros and cons. Toxicol Appl Pharmacol 2003;189:233–46.
[34] Vermeir M, Annaert P, Mamidi R, Roymans D, Meuldermans W, Mannens G. Cell-based models to study hepatic drug metabolism and enzyme induction in humans. Expert Opin Drug Metab Toxicol 2005;1:75–90.